Available online at www.sciencedirect.com

ScienceDirect

Geochimica et Cosmochimica Acta 198 (2017) 32–47

Geochimica et Cosmochimica Acta

www.elsevier.com/locate/gca

Tooth enamel maturation reequilibrates oxygen isotope compositions and supports simple sampling methods

Robin B. Trayler *, Matthew J. Kohn

Department of Geosciences, Boise State University, Boise, ID 83725, United States

Received 5 April 2016; accepted in revised form 14 October 2016; Available online 5 November 2016

Abstract

Oxygen isotope and major element zoning patterns of several disparate ungulate teeth were collected to evaluate the timing and geometry of enamel formation, records of isotope zoning, and tooth enamel sampling strategies. Isotopic zoning in mammalian tooth enamel encodes a sub-annual time series of isotopic variation of an animal's body water composition, with a damping factor that depends on the specifics of how enamel mineralizes. Enamel formation comprises two stages: precipitation of appositional enamel with a high CO_3:PO_4 ratio, followed by precipitation of maturational enamel with a lower CO_3:PO_4. If appositional and maturational enamel both contribute to isotope compositions (but with different CO_3:PO_4), and if isotope compositions vary seasonally, paired $\delta^{18}O$ values from CO_3 and PO_4 profiles should show a spatial separation. CO_3 isotope patterns should be shifted earlier seasonally than PO_4 isotope patterns. Such paired profiles for new and published data show no resolvable shifts, i.e. CO_3 and PO_4 $\delta^{18}O$ profiles show coincident maxima and minima. This coincidence suggests that enamel maturation reequilibrates appositional isotope compositions. If enamel maturation establishes enamel isotope compositions, the geometry of maturation, not apposition, should be considered when devising sampling protocols. X-ray maps of Ca zoning show that the majority of enamel (inner and middle layers) mineralizes heavily at a high angle to the external tooth surface and the enamel-dentine junction over length scales of 2–4 mm, while the outer enamel surface mineralizes more slowly. These data suggest that isotopic sampling strategies should parallel maturational geometry and focus on interior enamel to improve data fidelity. The magnitude of isotopic damping is also smaller than implied in previous studies, so tooth enamel zoning more closely reflects original body water isotopic variations than previously assumed.
Published by Elsevier Ltd.

Keywords: Stable isotopes; Enamel mineralization; Tooth growth; Maturation

1. INTRODUCTION

Stable isotopes in mammalian tooth enamel are commonly used to address a variety of ecological and climatological questions (e.g., see Koch, 1998, 2007; Kohn and Cerling, 2002; Clementz, 2012). Unlike bone and dentine, enamel is not strongly susceptible to diagenetic alteration, so it faithfully preserves biogenic isotope compositions over millions of years. Teeth also mineralize progressively from tooth tip to root and are not remodeled after formation, so they encode and preserve a sub-annual times series of isotopic variations in the animal. Subsampling to extract these variations has become a well established technique to investigate sub-annual fluctuations in climate and feeding ecology (e.g., Fricke and O'Neil, 1996; Fricke et al., 1998; Kohn et al., 1998; Balasse, 2002). However, because enamel formation consists of multiple discontinuous stages of mineralization, isotopic zoning within a tooth does not perfectly record the instantaneous isotope composition of an animal or environment, rather the record is damped relative to this variation (Passey and Cerling, 2002). Several authors have proposed approaches to minimize this

* Corresponding author.
E-mail address: robintrayler@boisestate.edu (R.B. Trayler).

http://dx.doi.org/10.1016/j.gca.2016.10.023
0016-7037/Published by Elsevier Ltd.

problem, either by subsampling strategies (Hoppe et al., 2004; Zazzo et al., 2012; Blumenthal et al., 2014; Holroyd et al., 2014) or by numerical modeling and inversion (Passey et al., 2002, 2005). Both these approaches rely on accurate understanding of the timing and geometry of enamel formation.

In this paper, we examine chemical and isotopic systematics in tooth enamel to critically evaluate how it forms and encodes its isotope composition. In the first part of the paper we show that while enamel forms via a two-stage process, only second stage mineralization appears to contribute to the isotope compositions recorded in teeth – compositions essentially reequilibrate during maturation so that the physical and isotopic character of first-stage mineralization appears inconsequential to isotope studies. In the second part we use X-ray composition mapping of several developing teeth to investigate the complexities of second-stage mineralization and its relationship to existing subsampling strategies. The geometry of second-stage mineralization bears little to no resemblance to first-stage mineralization. Consequently, even if apposition-stage isotopic compositions were partially preserved, proposed sampling strategies based on first-stage microstructure alone should be avoided.

2. ENAMEL MINERALOGY AND FORMATION

Enamel is the most highly mineralized tissue in mammals, and contains nearly 100% bioapatite mineral. Chemically, bioapatite is $Ca(PO_4)_3OH$ with carbonate (CO_3) substitutions in the phosphate (PO_4) and hydroxyl (OH) sites (Elliott, 2002). Both the carbonate and phosphate components are commonly analyzed for their stable isotope compositions. Of the two, carbonate analysis is more common, both because it archives two isotope systems, carbon and oxygen, and because analysis is simpler. Enamel phosphate is thought to be more resistant to diagenesis, leading to its use primarily on geologically older fossils (Kohn and Cerling, 2002).

Enamel microtexture in mammals is broken into two broad categories, radial and decussate enamel, distributed in three regions of enamel – outer, central, and inner regions – from the outer enamel surface (OES) to the enamel-dentine junction (EDJ). Radial enamel commonly forms the outer and inner enamel layers, although the inner layer varies in thickness (Pfretzschner, 1992; Koeingswald et al., 1993). In radial enamel, enamel prisms are oriented perpendicular to either the OES or EDJ. Decussate enamel prisms intersect and cross at shallow to high angles (crisscross) and bundle together to form optically distinct, macroscopically visible bands called Hunter-Schreger bands. Decussate enamel makes up the central and sometimes inner layers of enamel, and therefore, the majority of enamel volume in large mammals (Koenigswald and Sander, 1997; Moss-Salentijn et al., 1997).

Enamel mineralization takes place in two distinct stages, apposition (first-stage) and maturation (second-stage; Fig. 1; Robinson et al., 1978, 1979; Suga, 1979, 1982). Here we refer to the two correspondingly distinct mineral components as appositional and maturational bioapatite. During apposition, mineralization initiates at the occlusal or wear surface of the tooth and progresses toward the root. A protein matrix forms and is seeded with diffuse enamel crystallites (Fig. 1A). The surface of new apposition forms a low angle relative to the EDJ, such that sequential appositional layers imbricate. In fully mineralized enamel, incremental growth bands called striae of Retzius record the orientation of the appositional front (Hillson, 1986). The angle of apposition for several groups of ungulates is commonly ~5–15° relative to dentine (Kierdorf and Kierdorf, 1997; Hoppe et al., 2004; Kierdorf et al., 2006, 2012, 2013). The appositional matrix is mineral poor, with only ~25 wt% bioapatite (Moss-Salentijn et al., 1997; Passey and Cerling, 2002). While the total mineral content of the appositional matrix is low, however, appositional bioapatite within is carbonate rich, containing twice as much CO_3 as fully mature enamel (Robinson et al., 1979; Sydney-Zax et al., 1991). This difference in mineral content vs. CO_3 content is crucial to our study – if appositional bioapatite is retained in the final enamel, it contributes ~25% of the total mineral (PO_4) but ~50% of total CO_3. The innermost enamel layer, a 10–20 μm band along the EDJ, differs from this pattern of mineralization because it is heavily mineralized – at least 50% – early in enamel formation (Suga, 1979, 1982; Tafforeau et al., 2007; Blumenthal et al., 2014). Because this layer is so thin and rarely isolated for analysis, we do not consider its isotope systematics.

After apposition, enamel undergoes a prolonged maturation stage. Similar to apposition, maturation progresses from occlusal surface to root, although not necessarily at the same rate or with the same geometry (Fig. 1B, D). Maturation occurs earlier and faster in the inner and central enamel layers, with the outer enamel layer mineralizing last. During this stage, crystallites coarsen and infill, reducing organic contents to final concentrations of $\leqslant$1 wt% (Robinson et al., 1979; Suga, 1979, 1982; Hillson, 1986, 1978) and depositing the remaining ~75 wt% mineral and ~50 wt% of carbonate (Robinson et al., 1979; Sydney-Zax et al., 1991). While bulk enamel has a carbonate content of 3–4 wt% it is heterogeneously distributed ranging from ~5 wt% near the EDJ to ~3 wt% at the OES (Zazzo et al., 2005).

3. MODELING ENAMEL ISOTOPE COMPOSITIONS

If bulk enamel represents contributions from both appositional and maturational bioapatite, a bulk isotope composition should represent an average of their respective compositions, weighted by the amount contributed during each stage:

$$\delta_{final} = \delta_{app} \times f_{app} + \delta_{mat} \times (1 - f_{app}) \quad (1)$$

where δ_{final} = the final isotope composition of mature enamel, δ_{app} and δ_{mat} are the isotope compositions of appositional and maturational bioapatite respectively, and f_{app} is the fraction of the isotope deposited during apposition (Fig. 1C, E).

Passey and Cerling (2002) modeled this concept using two equations (see Table 1 for model parameters):

$$\delta_{ei} = (f_{app} \times \delta_{mi}) + (1 - f_{app}) \times \frac{\sum_{n=i+1}^{i+1+l_m} \delta_{m_n}}{l_m} \quad (2)$$

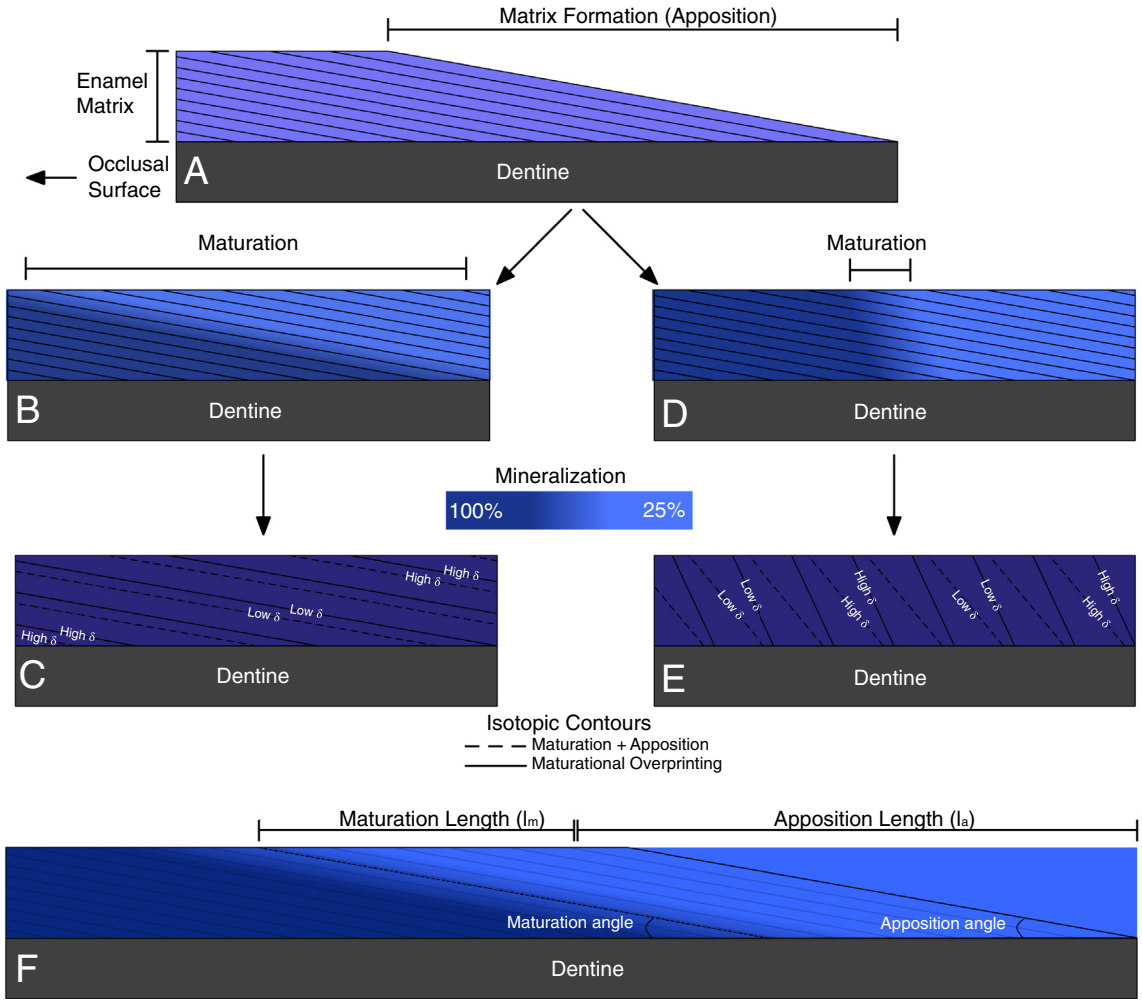

Fig. 1. Simplified schematic diagram showing two possible models of enamel formation. (A) Apposition initiates at the occlusal (wear) surface and progresses toward the root at a low angle relative to the enamel-dentine junction. (B, C) Maturation progresses through the matrix following the same geometry as apposition. The orientation of isotopic contours (dashed lines) parallels apposition. (D, E) maturation progresses through the matrix following a different geometry from apposition. The orientation of isotopic contours does not parallel apposition. Solid lines are the predicted isotopic contours if maturation re-equilibrates appositional mineral. (F) Relationship between Passey and Cerling (2002) model parameters and enamel mineralization.

Table 1
Model parameters for the Passey and Cerling (2002) model.

Parameter	Definition
δ_{ei}	Final isotope composition of mature enamel
f_{app}	Fraction of mineral formed during apposition
δ_{mi}	Isotope composition of enamel formed during apposition
δ_{m}	Isotope composition of enamel formed during maturation
l_m	Length scale of maturation
l_a	Length scale of apposition
δ_{ci}	Isotopic composition of a sampled column of enamel

$$\delta_{ci} = \frac{1}{l_a}\sum_{n=i-l_a}^{i}\delta_{e_n} \quad (3)$$

where δ_{ei} = the isotope composition at any point i, f_{app} is the decimal fraction of enamel formed during apposition, and δ_{ci} = the isotope composition of enamel at i, averaged over a column through the thickness of enamel. Eq. (2) implies that isotope compositions reflect a contribution from appositional bioapatite (first term on the right-hand side), and a time integrated contribution from maturational bioapatite over the length of maturation (second term on the right-hand side). The Passey and Cerling (2002) model makes four assumptions: (1) Maturation length (l_m) is constant (no variations in tooth enamel mineralization rate along the length of a tooth); (2) Maturation initiates immediately after apposition (no time lags between apposition and maturation); (3) The geometry of maturation parallels apposition (no variations in mineralization rate with depth, such as early mineralization of the central Hunter-Schreger bands); (4) both appositional and maturational bioapatite contribute to the final isotope composition of enamel (no resorption or recrystallization of appositional bioapatite).

Although the concentration of phosphate is virtually identical between appositional and maturational bioapatite, the concentration of carbonate differs systematically – there is about twice as much carbonate in appositional bioapatite as in fully formed enamel (Sydney-Zax et al., 1991). These differences imply that the oxygen isotope composition of carbonate vs. phosphate components should be weighted differently in Eq. (1). In both cases:

$$f_{app} = \frac{f_{mineral,app}}{f_{mineral,final}} \times \frac{\mathrm{wt\%_{i,app}}}{\mathrm{wt\%_{i,final}}} \quad (4)$$

where $f_{mineral,app}$ and $f_{mineral,mat}$ are the fractions of mineral in appositional and final (completely mature) enamel, respectively (normally 25% and 100%), and $\mathrm{wt\%_{i,app}}$ and $\mathrm{wt\%_{i,final}}$ are the weight percents of the component i in appositional and final bioapatite respectively. For phosphate $\mathrm{wt\%_{PO4,app}}$ and $\mathrm{wt\%_{PO4,final}}$ are virtually identical (e.g. Ca/P weight ratios are identical; Hiller et al., 1975; Sydney-Zax et al., 1991). So f_{app} follows mineral content: 25% appositional bioapatite would contribute 25% of the PO_4 in fully formed enamel. For carbonate however, $\mathrm{wt\%_{CO3,app}}$ is $\sim 2 \times \mathrm{wt\%_{CO3,final}}$, so 25% appositional bioapatite would contribute ~50% of the CO_3 in fully formed enamel. This in turn implies that the carbonate component of enamel is weighted toward an earlier period of enamel formation than the phosphate component and that seasonal variations in $\delta^{18}O$ should be recorded differently in CO_3 vs. PO_4 components.

We explored the quantitative implications of differing values of f_{app} for CO_3 and PO_4 using the Passey and Cerling (2002) model, assuming $f_{CO3,app} = 0.50$ and $f_{PO4,app} = 0.25$ (Fig. 2). We assumed published values for the length scales of maturation (l_m ~25 mm; Balasse, 2002) and apposition (l_a ~15 mm; Passey and Cerling, 2002). Because $f_{CO3} \neq f_{PO4}$ oxygen isotope zoning patterns in these components should be phase shifted relative to one another. Similarly, the oxygen isotope offset, $\Delta(CO_3–PO_4)$, measured between paired samples should vary systematically, which may help explain why reported $\Delta(CO_3–PO_4)$ values for enamel are not constant (Bryant et al., 1996; Fox and Fisher, 2001; Zazzo et al., 2004; Martin et al., 2008; Pellegrini et al., 2011).

Within the context of model predictions, and our overall goal of understanding how mineralization patterns affect isotope records, we addressed two specific questions:

First, are oxygen isotopes in the carbonate and phosphate components shifted relative to one another, as predicted. A phase shift, if present, implies that the two components record isotopes differently, which must be considered in interpreting PO_4 vs CO_3 isotope data. Conversely, the lack of a phase shift would imply that maturation overprints or re-equilibrates appositional mineral, removing its contribution to the bulk isotope composition of mature enamel.

Second, what is the geometry of enamel maturation? Since appositional enamel forms at a low angle relative to the EDJ, sampling perpendicular to the EDJ cross cuts weeks or months of appositional features (Holroyd et al., 2014). However, since maturation deposits 50% of carbonate and 75% phosphate, the orientation of mineralization is crucial to understanding how isotopes are recorded within a tooth. Additionally, the length scale of maturation strongly influences the degree to which isotope variations are damped (Eq. (2)).

4. MATERIALS AND METHODS

4.1. Stable isotopes

We selected five teeth for stable isotope analysis. Three teeth – horse (*Equus ferus caballus*), goat (*Capra hircus*), and bison (*Bison* sp.) – were fully mineralized and should reflect their post maturation isotopic compositions. For isotopic analyses we identified fully mature enamel based on hardness and texture. Immature enamel is soft (Passey and Cerling, 2002) with a fibrous texture and could be easily scraped from a tooth using a scalpel, while highly mineralized tissue required the use of a drill. We also selected two immature elk (*Cervus elaphus*) teeth. Since these teeth are partially mineralized, the isotopic input from maturation should be minimized over the region of apposition. Sampled teeth were cleaned with a carbide burr and rinsed with ethanol to remove surficial material before sampling. Serial samples were hand milled perpendicular to the growth axis using a Dremel® rotary tool and a 0.5 mm carbide dental drill bit. This resulted in 86 subsamples across the five teeth (see Appendix). Approximately 8 mg of enamel powder were pretreated using the approach of Koch et al. (1997). We first oxidized residual organics overnight using excess 30% hydrogen peroxide. The hydrogen peroxide was decanted and the powder was rinsed twice with deionized water. After rinsing, the powders were treated with a 1.0 M Ca-acetate – acetic acid buffer overnight to remove labile carbonates. After pretreatment the powders were rinsed three times with deionized water and dried in a vacuum oven at 40 °C. After pretreatment each sample was split and analyzed for both PO_4 and CO_3 oxygen isotopes.

The CO_3 component of enamel was analyzed by digestion in phosphoric acid using a 2010 ThermoFisher Gasbench II coupled with a Delta V Plus continuous flow isotope ratio mass spectrometer, located in the Stable Isotope Laboratory, Department of Geosciences, Boise State University. The PO_4 component was re-precipitated as Ag_3PO_4 using the following method. An ~1.0 mg aliquot of enamel powder was dissolved in 200 µL 0.5 M nitric acid over several hours. After the powder was fully dissolved the solution was neutralized by added 150 µL of 0.5 potassium hydroxide. 400 µL of 0.36 M potassium fluoride was added to precipitate calcium as calcium fluoride. The remaining liquid was the transferred to a clean centrifuge tube and reacted with 500 µL of silver amine solution (0.2 M silver nitrate, 0.5 M ammonium nitrate, 0.74 ammonium hydroxide) at 50 °C overnight to form Ag_3PO_4 (Bassett et al., 2007; O'Neil et al., 1994). The resulting precipitate was rinsed five times in deionized water and analyzed using the same mass spectrometer coupled with a ThermoFisher TC/EA. All CO_3 oxygen isotope compositions were standardized to Vienna Standard Mean Ocean Water (VSMOW) using the NBS-18 and NB-19 calcite standards. Analytical reproducibility was ±0.24‰ (NBS-18; ±2σ) and ±0.34‰

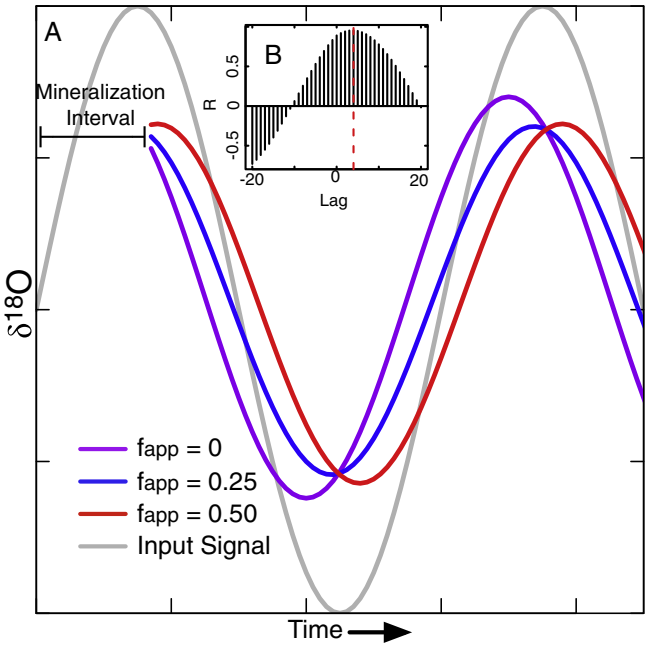

Fig. 2. (A) Modeled oxygen isotope compositions for enamel with different initial mineral fractions (f_{app}). Model outputs are phase shifted relative both to the input signal but also to model outputs with differing f_{app}. Therefore, $\delta^{18}O_C$ ($f_{app} = 0.50$; Sydney-Zax et al., 1991) should be a 1:1 mixture of appositional and maturational compositions while $\delta^{18}O_P$ ($f_{app} = 0.25$; Passey and Cerling, 2002) is more heavily weighted toward maturation. (B) Cross correlation between $f_{app} = 0.25$ and $f_{app} = 0.50$. Vertical red line indicates the lag associated with the highest correlation coefficient.

(NBS-19; $\pm 2\sigma$). Phosphate oxygen isotope compositions were standardized to VSMOW using the IAEA-601, IAEA-CH3 and IAEA-CH6 standards. Analytical reproducibility was ±0.44‰ (IAEA-601; $\pm 2\sigma$),±0.46‰ (IAEA-CH6; $\pm 2\sigma$), and ±0.56‰ (IAEA-CH3; $\pm 2\sigma$). Bioapatites and calcite acid fractionation factors exhibit systematic differences (Passey et al., 2007). To ensure consistent $\Delta(CO_3$–$PO_4)$ measurements between teeth we made small adjustments to our data based on repeated analysis of NIST-120c, a phosphorite with similar chemistry to bioapatite. Analytical reproducibility was ±0.47‰ (2σ) for the CO_3 component and ±0.73‰ (2σ) for the PO_4 component. We assume a phosphate $\delta^{18}O$ value of 21.7‰ (Chenery et al., 2010) and a carbonate $\delta^{18}O$ value of 28.5‰ (Kohn et al., 2015), and corrected our data to reflect a $\Delta(CO_3$–$PO_4)$ of 6.8‰ for concurrently analyzed NIST-120c. These corrections do not affect any of our interpretations. All isotope compositions are reported in the standard delta (δ) notation.

To investigate the predicted phase shifts between carbonate bound ($\delta^{18}O_C$) and phosphate bound ($\delta^{18}O_P$) oxygen isotope compositions, we treated our data as independent time series and calculated cross correlations between both data sets using R v3.1.2. Cross correlation determines the optimal alignment between two time series by repeatedly calculating a correlation coefficient while varying the lag between the two series (Fig. 2). This approach assumes a near constant mineralization rate and a regular sampling interval. The mean sampling interval (Δx) over all teeth is 2.08 ± 1.50 mm (mean $\pm 2\sigma$). The cross correlation approach expresses any lag as an integer number (n) of sampling intervals. Therefore, if $n = 2$ and $\Delta x = 2.08$ mm the lag will be identified as 4.16 mm. It is important to note that any lag predicted using the Passey and Cerling (2002) model represents the minimum possible lag because the model assumes that maturation initiates immediately after apposition (i.e. $\Delta t_{app\text{-}mat} = 0$). However, if maturation initiates some time after the cessation of apposition, as our X-ray maps imply (see below) $\Delta t_{app\text{-}mat} > 0$. This relationship implies that lags between carbonate and phosphate data should be larger than the model predicts, because appositional and maturational bioapatite are separated by a larger period of time.

Pellegrini et al. (2011) suggested that CO_3 oxygen isotope zoning shows greater attenuation than PO_4 isotope zoning. The authors used a t-test on the pooled standard deviations of $\delta^{18}O_C$ and $\delta^{18}O_P$ values calculated independently for each tooth. For example, an individual tooth (tooth "A") might exhibit standard deviations in $\delta^{18}O_P$ and $\delta^{18}O_C$ of σ_C and σ_P. These two values constitute a single pair for tooth A. A second tooth (tooth "B") would provide a second pair of σ_C and σ_P values. These pairs were calculated across all teeth and a t-test performed on pooled σ_C and σ_P. In addition to replicating this technique we also compared the variances of $\delta^{18}O_C$ and $\delta^{18}O_P$ values using F-tests. We set significance at $p < 0.05$ for both tests.

4.2. Major element distributions

Major element compositional distributions were measured across five teeth with forming enamel. Slices of enamel were removed from each tooth parallel to the growth axis, mounted on glass slides, and polished using 0.3 μm alumina. After polishing, enamel slices were gold

coated and imaged. Mule deer (*Odocoileus hemionus*) and cow (*Bos taurus*) X-ray maps were collected using a Cameca SX-50 electron probe housed in the Electron Microscopy Center, University of South Carolina. Guanaco (*Lama guanacoe*), sheep (*Ovis aries*), and horse (*Equus ferus caballus*) X-ray maps were collected using a Cameca SX-50 electron probe housed in the Department of Geological Sciences, Brigham Young University, Utah. For both instruments, operating conditions included an expanded beam (5–10 μm) and 15 kV accelerating voltage. We used stage mapping, a 200 nA beam current, pixel sizes of 15 μm, and count times of 50 ms/pixel, and collected all data using wavelength dispersive spectrometers.

We use calcium X-ray maps as a proxy for mineral content. The geometry of maturation appears in X-ray maps as a transition between the poorly mineralized appositional matrix (low X-ray intensity) and the fully mature enamel (high X-ray intensity). We calculated changes in relative calcium concentrations over a window that included both fully mature and immature enamel using ImageJ (Abràmoff et al., 2004). When a clear maturational boundary is present we define the angle of maturation as the angle measured from the EDJ, proximal to the occlusal surface.

5. RESULTS

5.1. Stable isotopes

Teeth display moderate to strong zoning in both $\delta^{18}O_P$ and $\delta^{18}O_C$ values (Fig. 3; Table 2). The single bison M^3 is the most strongly zoned with total variations of 11.1‰ and 9.8‰ for CO_3 and PO_4 oxygen isotope compositions (Fig. 3B). The two elk teeth have the smallest total variation of ~2.5‰ (Fig. 3D, E). In contrast to the results of Pellegrini et al. (2011) our results do not show a consistent attenuation of $\delta^{18}O_C$ values relative to $\delta^{18}O_P$ values. A *t*-test of the pooled intra-tooth standard deviations across all sampled teeth shows no significant difference between $\delta^{18}O_C$ and $\delta^{18}O_P$ values ($p = 0.08$). Likewise, an *F*-test of pooled data reveals no significant difference in variances ($p = 0.63$).

5.2. Phase shifts

Cross correlations between $\delta^{18}O_C$ and $\delta^{18}O_P$ values show no detectable lag between the two components (Table 2; Fig. 3F). We also performed statistical tests on data for 8 teeth originally reported in Pellegrini et al. (2011). In general, isotopic zoning in their data is lower than in teeth sampled for this study, and subsample spacing is also higher (2.7 ± 2.0 mm; mean $\pm 2\sigma$). These considerations reduce the reliability of calculated lags. Four teeth indicate zero lag, whereas two teeth suggest a small positive lag and two teeth a small negative lag.

5.3. Compositional mapping

X-ray maps of relative calcium concentrations in immature and mature enamel reveal key mineralization details (Fig. 4). Appositional enamel is highly porous, and maturation reduces porosity. The heavily mineralized innermost enamel layer occurs as a thin band separating dentine from the majority of enamel and is barely visible at the resolution of these images. With the exception of *Bos taurus* visible calcium zones at the boundary between mature and immature enamel are oriented at high (>45°) oblique angles relative to the EDJ (Fig. 4A–D). This zoning defines the orientation of the maturation front. *Odocoileus* and *Lama* have similar maturation angles of ~60° (Fig. 4A, B), while the *Ovis* maturation angle is steeper (~80°; Fig. 4D). Unlike the results of Hoppe et al. (2004) who suggest that maturation in horses takes place at a low angle, calcium zoning in the sampled horse is oriented approximately perpendicular to dentine (~90°; Fig. 4C)). Each of these teeth also has a distinctive outer enamel "shelf" such that the innermost ~3/4 of enamel is heavily mineralized while the outermost enamel layer is more weakly mineralized. Contrasting with the relatively simple geometry of the other teeth, chemical maps in *Bos* enamel (Fig. 4E) reveal a maturation "wedge" or "plume" with the apex of the wedge falling apically about midway between the OES and EDJ, i.e. centered within the region of decussate enamel and Hunter-Schreger bands.

Compositional profiles (Fig. 5) show marked decreases in calcium concentrations across the maturation front. Transitions from high (mature) to low (immature) concentrations occur over a length scale of 2–4 mm in *Equus*, *Ovis*, *Lama* and *Odocoileus* (Fig. 5A–D) as determined by measuring the distance between the points of maximum curvature on plots of composition vs. distance. This transition is more protracted in *Bos* (Fig. 5E), with the profile rapidly reaching ~80% mineralization over a ~4 mm interval and then gradually increasing over ~6 mm to its maximum mineralization.

6. DISCUSSION

6.1. Lack of phase shifts between $\delta^{18}O_C$ and $\delta^{18}O_P$

Of the 13 teeth considered, 9 have no detectable lag between $\delta^{18}O_C$ and $\delta^{18}O_P$, including all new data collected in this study. And while re-analysis of teeth from Pellegrini et al. (2011) reveals small lags, the detected lags are not consistent, with small negative lags detected in two teeth and small positive lags in two others. With the exception of sample STCE, teeth with calculated lags have the lowest correlation coefficients and smallest oxygen isotope variation, so are most susceptible to analytical errors or other sources of noise. Because the detected lags are inconsistent we cannot explain these results as arising from a physiological process. Preferential diagenetic alteration of the CO_3 component might explain these anomalies. In general, isotopic exchange between enamel and fluid should shift the mean isotopic value and attenuate the overall range, but not phase shift. However, phase shifts in $\delta^{18}O_C$ compositions are possible if CO_3 is preferentially removed from different crystallographic sites (Roche et al., 2010) and if the sites are differentially filled during apposition or maturation. Because we do not know whether different sites are

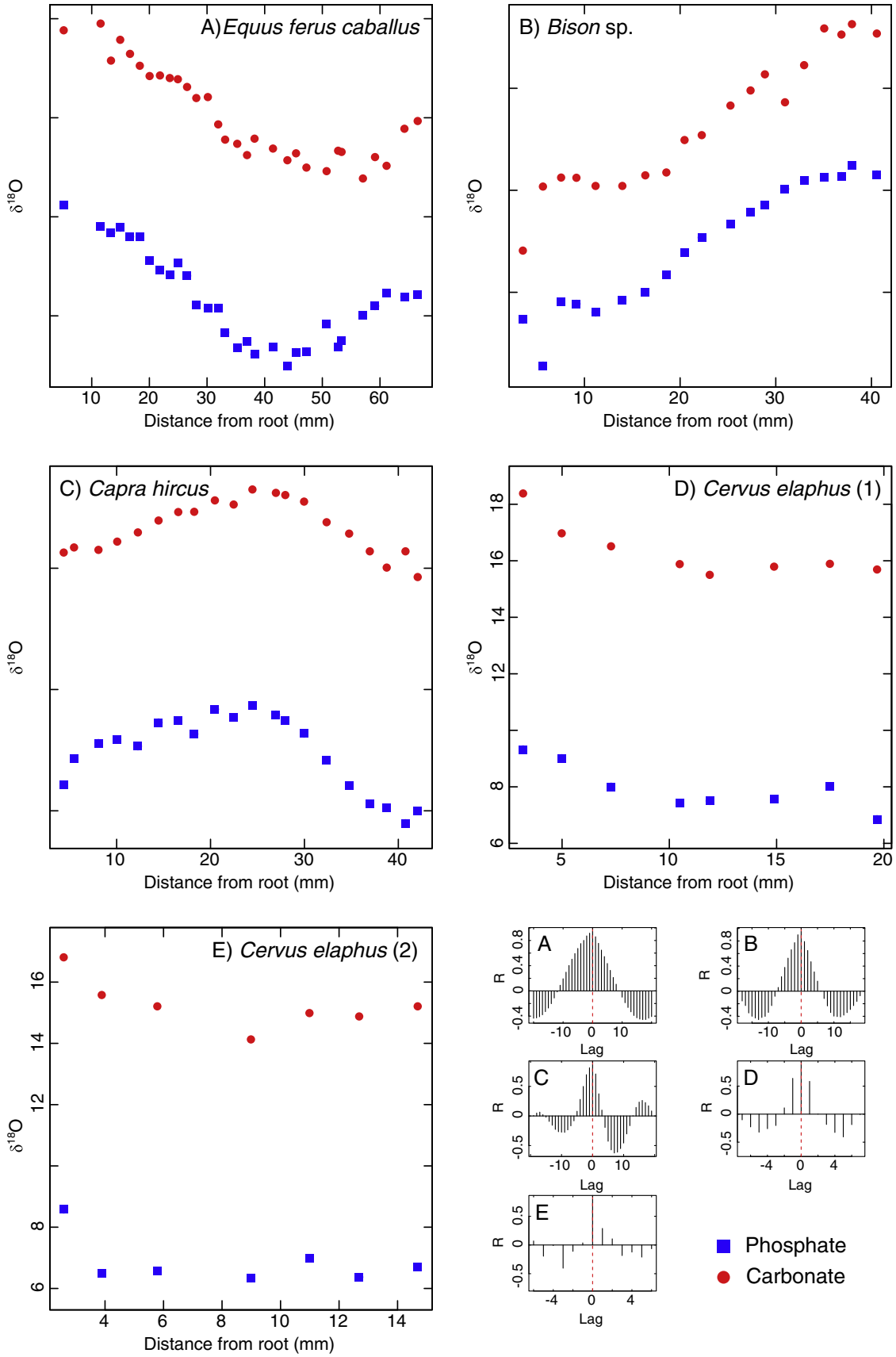

Fig. 3. Plots of paired CO_3 and PO_4 $\delta^{18}O$ values and their corresponding cross correlations. See Table 2 for descriptive statistics for each tooth. (A) *Equus ferus caballus*, (B) *Bison* sp., (C) *Capra hircus*, (D) *Cervus elaphus* (M-00-49), (E) *Cervus elaphus* (M-00-59).

Table 2
Descriptive statistics for tooth stable isotope data.

Taxa/sample	*n*	Subsample spacing Mean ± 1σ (mm)	Mean $\delta^{18}O_P$ (‰)	Range $\delta^{18}O_P$ (‰)	Mean $\delta^{18}O_C$ (‰)	Range $\delta^{18}O_C$ (‰)	$\Delta(CO_3$–$PO_4)$ ±1σ (‰)	Best lag	*R*
Equus ferus caballus	32	2.1 ± 1.0	11.0	8.1	20.1	7.8	9.3 ± 1.1	0	0.95
Bison sp. (28150)[1]	19	2.0 ± 0.5	12.3	9.8	18.2	11.1	5.9 ± 1.2	0	0.96
Capra hircus	20	2.0 ± 0.4	12.5	3.6	21.6	4.9	9.1 ± 0.8	0	0.87
Cervus elaphus (M-00-49)	8	2.4 ± 0.6	6.0	2.5	14.3	2.9	8.3 ± 0.4	0	0.89
Cervus elaphus (M-00-59)	7	2.0 ± 0.6	6.9	2.3	15.2	2.7	8.3 ± 0.4	0	0.8
Cervus elaphus (CACE)[a,b]	8	1.9 ± 0.1	17.9	2.8	27.2	2.3	9.3 ± 0.2	0	0.99
Cervus elaphus (PLCE)[a,b]	9	2.2 ± 0.2	17.7	2.9	26.6	3.0	9.0 ± 0.4	0	0.99
Cervus elaphus (STCE)[a,b]	6	2.4 ± 0.4	18.5	1.5	27.6	1.5	9.1 ± 0.5	−1	0.95
Cervus elaphus (PZCE)[a,b]	10	2.0 ± 0.3	17.2	3.5	26	3.2	8.9 ± 0.4	0	0.98
Equus hydruntinus (PZEH)[a,b]	15	3.0 ± 0.5	15.9	2.4	24.5	1.0	8.6 ± 0.6	1	0.6
Equus hydruntinus (STEH)[a,b]	12	4.8 ± 1.2	18.7	1.0	27.5	0.9	8.8 ± 0.4	−1	0.68
Equus hydruntinus (VAEH)[a,b]	36	2.3 ± 0.4	18.4	2.7	27.1	2.0	8.8 ± 0.4	0	0.84
Equus hydruntinus (PLEH)[a,b]	22	3.0 ± 0.9	17.7	2.9	26.7	1.2	9.0 ± 0.5	1	0.83

[a] Late Pleistocene.
[b] Data from Pellegrini et al. (2011).

filled during different stages of growth, such a view is at present speculative.

Why do highly zoned teeth fail to show phase shifts? Possible explanations include:

(1) The growth rate of the teeth is sufficiently rapid that no lag is resolvable.

The magnitude of a lag is related to the growth rate of the tooth. For example, ever growing rodent teeth have rapid enamel growth rates of ~150–440 mm/yr implying a very small time period of c. 2 weeks between the start of apposition and the end of maturation (see Kohn, 2004). In this case our methods probably would not resolve any lag between $\delta^{18}O_C$ and $\delta^{18}O_P$. Conversely, enamel growth rates for ungulates are ~30–60 mm/yr (Kohn, 2004). Model predictions for these teeth imply minimum lags of ~1–2 months between $\delta^{18}O_C$ and $\delta^{18}O_P$ values, or physical offsets of ~2.5–5 mm. Such offsets should be resolvable from our data suggesting some other explanations.

(2) Enamel mineral may re-equilibrate during maturation either by recrystallization and exchange of appositional mineral or by oxygen isotope diffusion between enamel and body fluids. Zazzo et al. (2010) investigated the contribution of appositional CO_3 to the final enamel carbon isotope composition using carbon isotope from the teeth of sheep that were switched between a diet of C_3 and C_4 plants. The authors fit the Passey and Cerling (2002) model to serially sampled $\delta^{13}C$ values, while varying the value of f_{app}. Values of f_{app} of either 0.0 or 0.50 produced the best model fits suggesting that at least a partial re-equilibration of carbon isotopes is possible. For this process to occur, however, some mechanism for preserving appositional features is required. For example, incremental structures and fluorescent labels with appositional geometries are observed in mature enamel (Kierdorf et al., 2013). How are these preserved?

For physical structures, inasmuch as mineral replacement reactions are often pseudomorphic (Putnis, 2002), appositional structures might be preserved even as appositional crystals are replaced and isotopically reequilibrate. Consideration of the chemical process of maturation implies that that mineral-bound fluorescent labels should be preserved. Calcium concentrations in body fluids are low (~40 ppm; Driessens and Verbeeck,1990), implying Ca enrichment factors of $\sim 10^4$ between bioapatite and serum. Thus, enamel serves as a highly effective Ca sink, limiting any exchange of Ca between enamel and serum. Any Ca in serum at the site of enamel maturation is simply scavenged into new-formed crystals. This process severely limits the potential for any Ca or Ca-chelating labels to leave the maturation site. Even so, some post appositional mobility is observed as fluorescent labels and radiophosphorous distributions broaden during maturation (Robinson et al., 1974; cf. Fig. 1, Kierdorf et al., 2013).

Diffusional exchange would also preserve physical structures. Although intracrystalline diffusion rates in apatite are slow (Cherniak, 2000), faster diffusion rates are possible in the near surface region of minerals (Stipp et al., 1992). For crystallites with a sufficiently high surface area to volume ratio, such as bioapatite, this effect could allow rapid diffusional exchange on a whole crystal scale (Kohn, 2008).

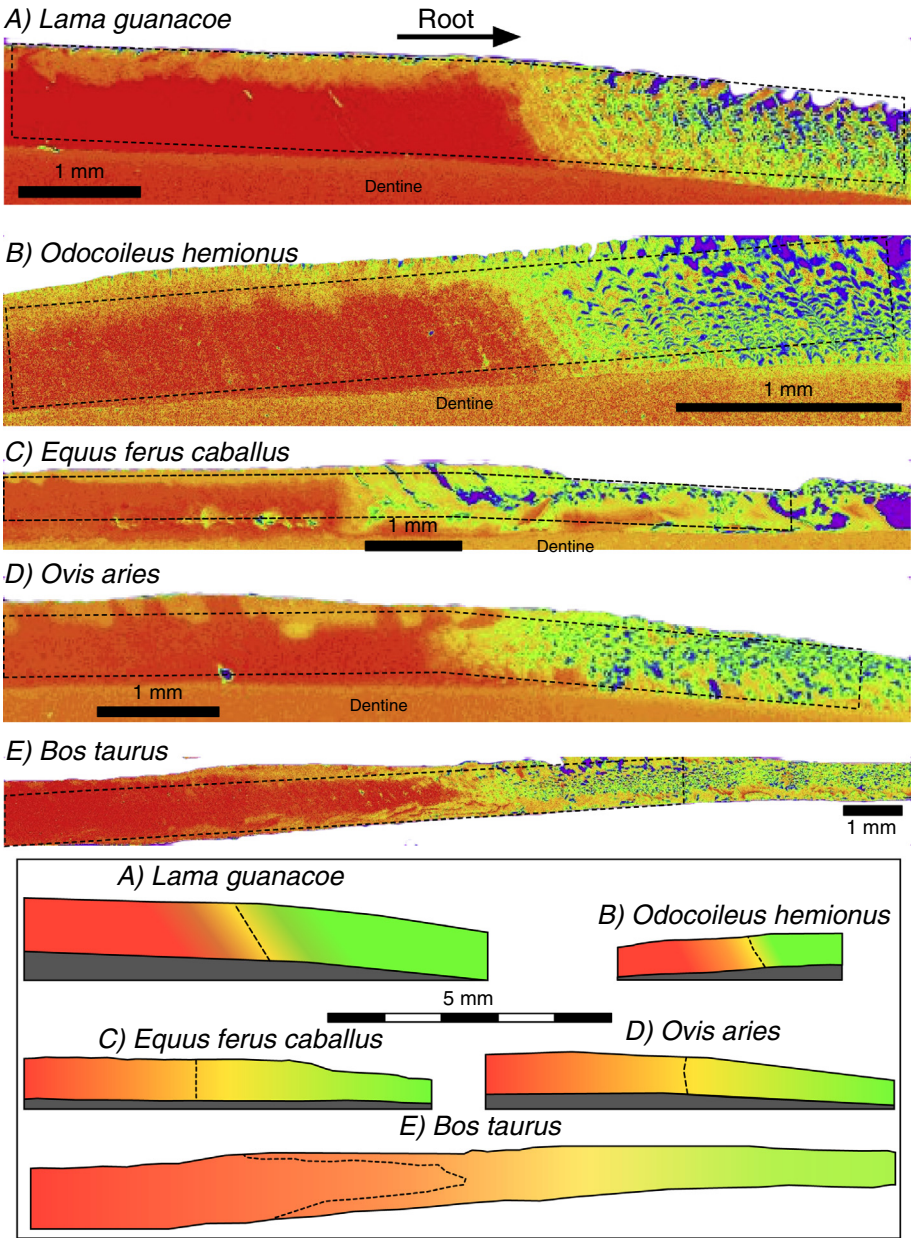

Fig. 4. X-ray maps of calcium zoning for teeth with both mature (occlusal) and immature (apical) enamel. (A) *Lama guanacoe*, (B) *Odocoileus hemionus*, (C) *Equus ferus caballus*, (D) *Ovis aries*, (E) *Bos taurus*. Warm colors indicate higher relative concentrations; blue/purple = pore space. Dashed boxes indicate areas over which calcium concentration profiles were plotted (Fig. 5). Box: schematic representations of enamel formation with inferred angles of maturation (dashed line). (For interpretation of the references to color in this figure legend, the reader is referred to the web version of this article.)

Since serum is composed primarily of water, the reservoir of exchangeable oxygen is more than sufficient to reset oxygen isotope compositions during maturation. Low Ca concentrations in serum, however, imply that Ca exchange and alteration of fluorescent labels would be limited.

6.2. Geometry of enamel maturation

Enamel apposition occurs at a consistently low angle relative to the EDJ in horses (Hoppe et al., 2004). Various labeling techniques record similarly shallow appositional angles in sheep, cows, and deer (Kierdorf and Kierdorf, 1997; Kierdorf et al., 2006, 2012, 2013), as do trace element distributions in primate enamel (Austin et al., 2013). However, our compositional maps clearly show that the geometry of enamel maturation may be complex and is independent of appositional geometry. An important implication is that incremental features that record appositional geometries, such as striae of Retzius, do not indicate either the geometry of maturation (Fig. 4) or the distribution of isotopes within the enamel. Inasmuch as most enamel mineralizes during maturation, not apposition, sampling

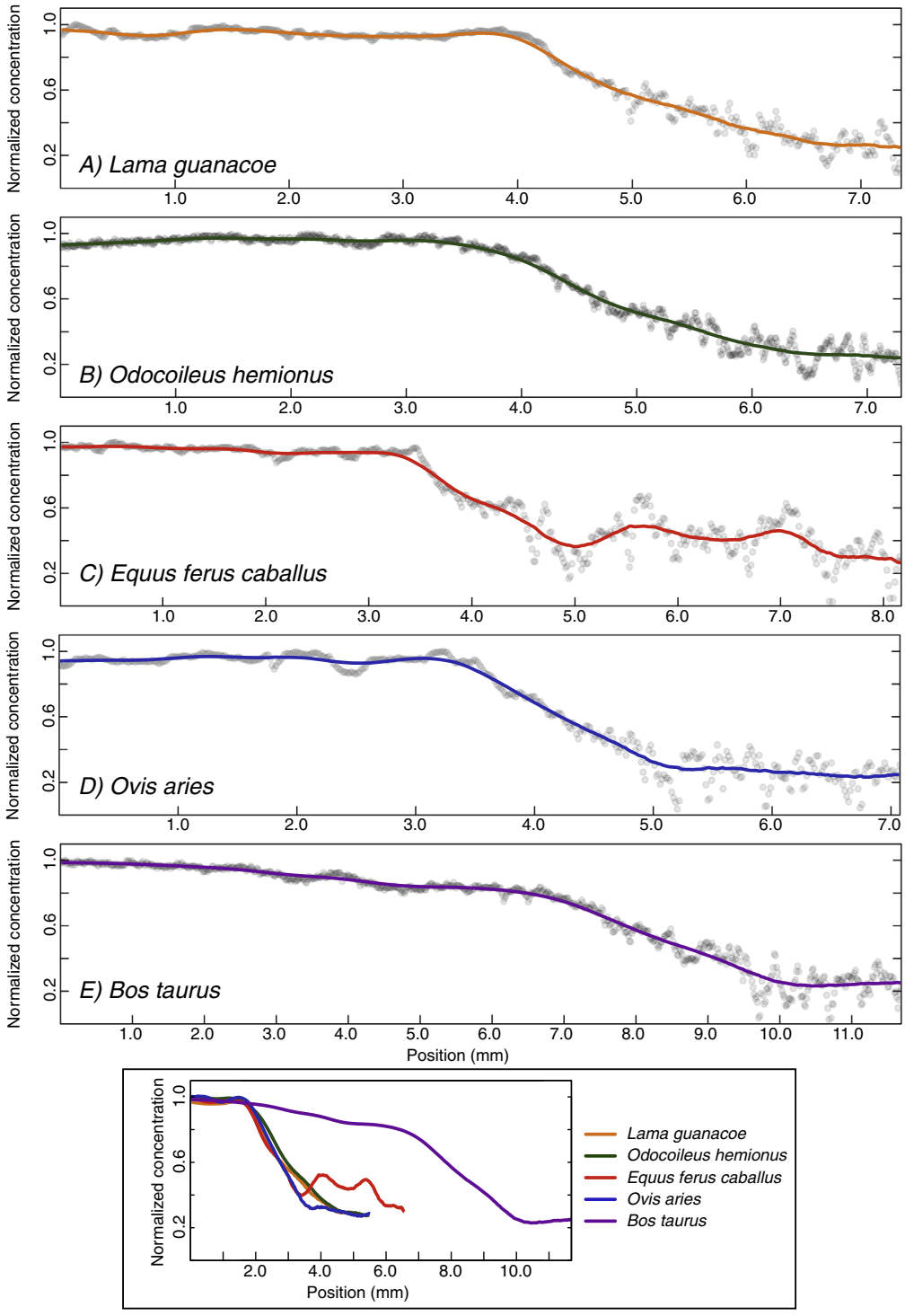

Fig. 5. Relative calcium compositional profiles along the dashed boxes in Fig. 4. (A) *Lama guanacoe*, (B) *Odocoileus hemionus*, (C) *Equus ferus caballus*, (D) *Ovis aries*, (E) *Bos taurus*. Concentrations were normalized using a linear transformation such that fully mature enamel and appositional enamel reflect mineralization fractions of 1.0 and 0.25 respectively. Box: Smoothed curves plotted with the same distance scale and shifted so the points of maximum curvature align. In all cases the transition from high to low calcium concentrations occurs over a length scale of 2-4 mm.

strategies based on incremental features alone will be invariably flawed and should be avoided.

Our data agree with complementary observations for diverse taxa that show that the outer enamel layer mineralized later than the inner and center enamel layers (Suga, 1982; Blumenthal et al., 2014). The outer enamel "shelf" appears to make up about a quarter of the total enamel volume. Its late mineralization implies that it should

record a later period of time relative to the inner and central layers. Data for a cow whose diet was switched from pure C_3 plants (enamel $\delta^{13}C$ ~12‰) to pure C_4 plants (enamel $\delta^{13}C$ ~0‰; Zazzo et al., 2005) support this inference (Fig. 6). The dietary switch caused the cow's $\delta^{13}C$ to increase through time. Microsamples through the thickness of enamel show higher $\delta^{13}C$ values for the outer ~0.3 mm of enamel, relative to interior enamel. A reversal in isotope composition is evident in the center of one profile, and suggests that the central (decussate) enamel mineralized earlier than radial enamel on either side. This mineralization behavior is consistent with the "wedge" of mineralization that we imaged in our cow enamel (Fig. 4E).

Possible textural differences (radial vs. decussate) and location (nearer the EDJ vs. nearer the OES) combine to influence the timing of enamel maturation. For example, if enamel had a consistent texture throughout its thickness it might mineralize with a simple planar geometry: earliest at the EDJ, at some intermediate time in the middle of enamel and last at the OES. The model of Passey and Cerling (2002) mimics this pattern. If decussate enamel experiences earlier and more rapid mineralization, however, a more complex geometry results in which radial enamel near the EDJ could mineralize at the same time or even later than decussate enamel in the middle followed last by radial enamel near the OES. This view qualitatively explains some features of the compositional maps (Fig. 4, especially *Lama*, *Odocoileus* and *Bos*) but whether it applies across enamel types and animal groups requires further investigation.

Generalized models require estimates of l_m which is rare. Passey and Cerling (2002) estimated l_m for *Hippopotamus amphibius* (~65 mm), *Bos taurus* (~15 mm), and *Bison bison* (~25 mm), based on bulk phosphorus content for samples milled perpendicular to the growth axis. This technique integrates a column of enamel into a single sample, however, so it is unable to resolve geometric complexities in enamel maturation. Using backscattered electron imagery of an *Equus* (horse) tooth, Blumenthal et al. (2014) estimated l_m of the inner and central enamel layers as ~28 mm. Their maturation trends are non-linear however, and ~60% of new enamel mass is added to appositional enamel over a much shorter distance, reaching 80–90% of final bioapatite mineral in <10 mm. If this rapid initial stage of maturation (representing ~60% of final bioapatite mass) isotopically resets appositional bioapatite (representing 25% of final bioapatite mass), 80–90% of the isotope composition is established over a short distance and correspondingly short period of time.

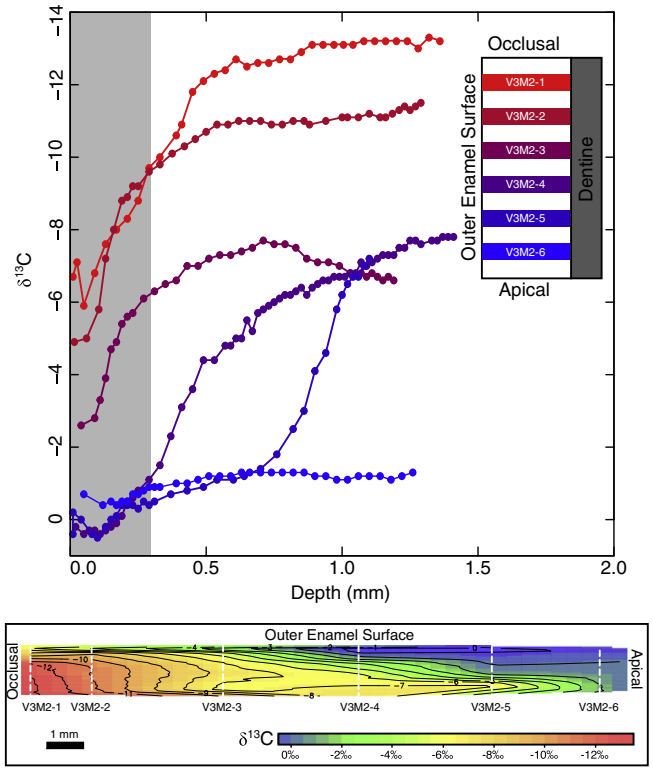

Fig. 6. Carbon isotope compositions (note reversed axis) versus depth from outer enamel surface for slices of *Bos taurus* enamel (After Zazzo et al., 2005). The animal was switched from a pure C_3 to pure C_4 plant diet to induce a large change in its carbon isotope composition. Gray bar indicates the outermost 0.3 mm of enamel, approximately the thickness of the outer enamel shelf observed on our compositional map of *Bos taurus* enamel (Fig. 4). The outer enamel layer is compositionally biased by the dietary shift to C_4 plants, suggesting later mineralization. Box: Interpolated carbon isotope compositions based on the six depth profiles of Zazzo et al. (2005). Carbon isotope contours suggest late mineralization for the outer enamel surface, while mineralization of the inner enamel layer progresses more rapidly. Vertical dashed lines indicate sample locations. Contour interval is 1‰.

Bendrey et al. (2015) proposed an exponentially decreasing growth rate in horse molars. Similarly, Kierdorf et al. (2013) report a decreasing mineralization rate near the enamel-root contact for sheep molars. Both these models imply rapid, near-linear growth rates for the majority (~80% of total length) of enamel, with a rapid decrease in mineralization rate near the enamel-root contact Our samples nearly all fall outside the near root region of the tooth where mineralization rates slow. Therefore, our estimates of maturation duration should represent a near maximum maturation rate. Rapid maturation implies a relatively small value of l_m and substantially decreases the magnitude of isotopic damping (Eq. 2; Passey and Cerling, 2002). That is, depending on the specifics of maturation geometry and rate, tooth enamel may preserve an isotopic record of an animal's body composition with higher fidelity than other studies (e.g. Kohn, 2004) have inferred.

6.3. Implications for subsampling

Our observations show that the inner and central enamel layers mineralize heavily over a length scale of 2–4 mm. The outermost layer mineralizes later, but makes up only ~25% of the total enamel thickness. Therefore, a majority of enamel mineralizes over a relatively short length. Since enamel growth rates are known or inferable from isotope zoning for many taxa (Kohn, 2004), the maturation length can be converted to time simply by dividing by the growth rate. Yearly mineralization rates vary among taxa but are commonly 30–60 mm/year for ungulates (Kohn, 2004). Therefore, a length scale of maturation of 2–4 mm equates to a maturation rate for the inner and central enamel of 1/2 to 1 1/2 months. The length scale of mineralization for the outermost enamel is much more poorly known, but backscattered electron images of horse enamel suggest it is at least 2 times the length scale for the inner enamel (Blumenthal et al., 2014). These sparse data suggest a maturation rate of at least 1–3 months.

Several studies have proposed strategies to reduce the damping associated with progressive mineralization. Hoppe et al. (2004) suggest milling along low-angle striae of Retzius, parallel to appositional microtextures. Maturation clearly does not follow appositional geometry in any of the diverse taxa we studied. The high angle commonly observed between the maturation front and the EDJ suggests that milling at a low angle averages more than simple perpendicular sampling and degrades seasonal signals. Cerling and Sharp (1996) used *in situ*, laser ablation to analyze fossil enamel $\delta^{13}C$ and $\delta^{18}O$ values. Similarly, Blumenthal et al. (2014) used secondary ion mass spectrometry to collect $\delta^{18}O$ values from the highly mineralized innermost enamel layer. While these *in situ* methods offer micron scale spatial resolution, they incorporate oxygen isotopes from three possible sources: hydroxyl, phosphate, and carbonate. The hydroxyl site is especially subject to diagenesis, so while bulk *in situ* analysis may be acceptable for modern specimens, its use on fossils may skew results, perhaps by as much as 1‰ (Kohn et al., 1999). Furthermore, models that link tooth enamel and drinking water isotope compositions make predictions for either the PO_4 component or CO_3 component, not bulk analysis of all oxygen bearing species.

By far the most common method of sampling enamel for stable isotope analysis is the use of a handheld dental drill or similar tool to mill samples perpendicular to the EDJ. This technique preferentially samples the outer and middle enamel layers, combining enamel from partially separated periods of mineralization. Carbon isotope depth profiles (Fig. 6; Zazzo et al., 2005) clearly show that the outer enamel layer records time shifted isotope values, while the inner and central layers preserve isotope "contours" nearly perpendicular to the EDJ. Selectively targeting central and inner enamel, either through micro-milling (i.e. Zazzo et al., 2005) or bulk removal of the outer enamel layer may reduce damping of isotope values associated with enamel maturation.

7. CONCLUSIONS

New and previously published oxygen isotope data show that carbonate and phosphate components of enamel record the same period of time, without a spatial or temporal lag, contrasting with current models. We suggest that enamel maturation isotopically reequilibrates the oxygen isotope composition of appositional bioapatite. In principle reequilibration should affect carbon isotopes as well, since carbon concentrations in serum are high. The effect on other commonly analyzed enamel components (i.e. trace elements) is unclear, although the persistence of Ca-binding labels in mature enamel suggest that little re-equilibration takes place in this case. X-ray chemical maps demonstrate that the inner and central enamel layers mineralize before the outermost enamel, dominantly over a narrow interval of 2–4 mm. These inner layers also mineralize at a high angle relative to the EDJ. Since maturation precipitates the majority of enamel bioapatite, and may isotopically reset some components, isotope sampling strategies should preferentially mimic maturational, not appositional geometries; we also recommend physically removing the outer enamel layer prior to sampling, or otherwise focusing on inner enamel whenever possible.

ACKNOWLEDGEMENTS

Funding was provided through NSF (United States) grants EAR-1349749 and EAR-1251443. We thank Dr. Samantha Evans and Dr. Samuel Matson for their help with isotopic analyses and Dr. Michael Dorais for help with electron probe analyses. We also thank Antoine Zazzo, Daniel Green, and one anonymous reviewer for their helpful comments.

APPENDIX A.

Table A1
Stable isotope data from all sampled teeth. IMHM = Idaho Museum of Natural History. BSU = Boise State University. Superscript and subscript indicate upper or lower tooth, respectively.

Taxa	Collection	Tooth	Position (mm)	$\delta^{18}O_P$	$\delta\ ^{18}O_C$
Bison sp.	IMHM 28150	M^3	3.6	8.7	12.0
Bison sp.	IMHM 28150	M^3	5.7	6.5	15.1
Bison sp.	IMHM 28150	M^3	7.6	9.6	15.6
Bison sp.	IMHM 28150	M^3	9.2	9.5	15.6
Bison sp.	IMHM 28150	M^3	11.2	9.1	15.2
Bison sp.	IMHM 28150	M^3	14.0	9.7	15.2
Bison sp.	IMHM 28150	M^3	16.4	10.1	15.7
Bison sp.	IMHM 28150	M^3	18.6	10.9	15.8
Bison sp.	IMHM 28150	M^3	20.5	12.0	17.4
Bison sp.	IMHM 28150	M^3	22.3	12.7	17.7
Bison sp.	IMHM 28150	M^3	25.3	13.4	19.1
Bison sp.	IMHM 28150	M^3	27.4	14.0	19.9
Bison sp.	IMHM 28150	M^3	28.9	14.3	20.6
Bison sp.	IMHM 28150	M^3	31.0	15.1	19.3
Bison sp.	IMHM 28150	M^3	33.0	15.6	21.1
Bison sp.	IMHM 28150	M^3	35.1	15.7	22.9
Bison sp.	IMHM 28150	M^3	36.9	15.8	22.6
Bison sp.	IMHM 28150	M^3	38.0	16.3	23.1
Bison sp.	IMHM 28150	M^3	40.6	15.8	22.6
Equus ferus caballus	BSU	M_3	5.2	15.7	24.4
Equus ferus caballus	BSU	M_3	11.6	14.6	24.7
Equus ferus caballus	BSU	M_3	13.4	14.2	22.8
Equus ferus caballus	BSU	M_3	15.0	14.5	23.9
Equus ferus caballus	BSU	M_3	16.7	14.1	23.2
Equus ferus caballus	BSU	M_3	18.4	14.1	22.6
Equus ferus caballus	BSU	M_3	20.1	12.9	22.1
Equus ferus caballus	BSU	M_3	21.9	12.4	22.1
Equus ferus caballus	BSU	M_3	23.6	12.1	22.0
Equus ferus caballus	BSU	M_3	25.0	12.7	21.9
Equus ferus caballus	BSU	M_3	26.6	12.1	21.5
Equus ferus caballus	BSU	M_3	28.2	10.6	21.0
Equus ferus caballus	BSU	M_3	30.2	10.5	21.0
Equus ferus caballus	BSU	M_3	32.0	10.4	19.6
Equus ferus caballus	BSU	M_3	33.2	9.2	18.9
Equus ferus caballus	BSU	M_3	35.3	8.5	18.6
Equus ferus caballus	BSU	M_3	37.0	8.8	18.1
Equus ferus caballus	BSU	M_3	38.3	8.1	18.9
Equus ferus caballus	BSU	M_3	41.5	8.5	18.4
Equus ferus caballus	BSU	M_3	44.0	7.5	17.8
Equus ferus caballus	BSU	M_3	45.5	8.2	18.2
Equus ferus caballus	BSU	M_3	47.3	8.3	17.4
Equus ferus caballus	BSU	M_3	50.8	9.6	17.3
Equus ferus caballus	BSU	M_3	52.8	8.5	18.3
Equus ferus caballus	BSU	M_3	53.4	8.8	18.2
Equus ferus caballus	BSU	M_3	57.1	10.1	16.9
Equus ferus caballus	BSU	M_3	59.2	10.6	18.0
Equus ferus caballus	BSU	M_3	61.2	11.2	17.5
Equus ferus caballus	BSU	M_3	64.3	11.0	19.4
Equus ferus caballus	BSU	M_3	66.6	11.1	19.8
Capra hircus	BSU	M_3	4.4	11.1	20.6
Capra hircus	BSU	M_3	5.5	12.2	20.8
Capra hircus	BSU	M_3	8.1	12.9	20.7
Capra hircus	BSU	M_3	10.1	13.0	21.1
Capra hircus	BSU	M_3	12.3	12.7	21.4
Capra hircus	BSU	M_3	14.5	13.7	21.9
Capra hircus	BSU	M_3	16.6	13.8	22.3
Capra hircus	BSU	M_3	18.3	13.2	22.3
Capra hircus	BSU	M_3	20.5	14.2	22.8
Capra hircus	BSU	M_3	22.5	13.9	22.6
Capra hircus	BSU	M_3	24.5	14.4	23.2

(*continued on next page*)

Table A1 (*continued*)

Taxa	Collection	Tooth	Position (mm)	$\delta^{18}O_P$	$\delta\ ^{18}O_C$
Capra hircus	BSU	M_3	27.0	14.0	23.1
Capra hircus	BSU	M_3	28.0	13.8	23.0
Capra hircus	BSU	M_3	30.0	13.2	22.7
Capra hircus	BSU	M_3	32.4	12.1	21.9
Capra hircus	BSU	M_3	34.8	11.1	21.4
Capra hircus	BSU	M_3	37.0	10.4	20.7
Capra hircus	BSU	M_3	38.8	10.2	20.0
Capra hircus	BSU	M_3	40.8	9.5	20.7
Capra hircus	BSU	M_3	42.1	10.1	19.6
Cervus elaphus (1)	BSU M-00-49	M_3	3.2	7.4	16.4
Cervus elaphus (1)	BSU M-00-49	M_3	5.0	7.1	14.9
Cervus elaphus (1)	BSU M-00-49	M_3	7.3	6.1	14.5
Cervus elaphus (1)	BSU M-00-49	M_3	10.5	5.5	13.9
Cervus elaphus (1)	BSU M-00-49	M_3	11.9	5.6	13.5
Cervus elaphus (1)	BSU M-00-49	M_3	14.9	5.6	13.8
Cervus elaphus (1)	BSU M-00-49	M_3	17.5	6.1	13.9
Cervus elaphus (1)	BSU M-00-49	M_3	19.7	4.9	13.7
Cervus elaphus (2)	BSU M-00-59	M_3	2.6	8.7	16.8
Cervus elaphus (2)	BSU M-00-59	M_3	3.9	6.6	15.6
Cervus elaphus (2)	BSU M-00-59	M_3	5.8	6.7	15.2
Cervus elaphus (2)	BSU M-00-59	M_3	9.0	6.4	14.1
Cervus elaphus (2)	BSU M-00-59	M_3	11.0	7.1	15.0
Cervus elaphus (2)	BSU M-00-59	M_3	12.7	6.4	14.9
Cervus elaphus (2)	BSU M-00-59	M_3	14.7	6.8	15.2

REFERENCES

Abràmoff M. D., Magalhães P. J. and Ram S. J. (2004) Image processing with ImageJ. *Biophoton. Int.* **11**, 36–43.

Austin C., Smith T. M., Bradman A., Hinde K., Joannes-Boyau R., Bishop D., Hare D. J., Doble P., Eskenazi B. and Arora M. (2013) Barium distributions in teeth reveal early-life dietary transitions in primates. *Nature* **498**, 216–219.

Balasse M. (2002) Reconstructing dietary and environmental history from enamel isotopic analysis: time resolution of intra-tooth sequential sampling. *Int. J. Osteoarchaeol.* **12**, 155–165.

Bassett D., Macleod K. G., Miller J. F. and Ethington R. L. (2007) Oxygen isotopic composition of biogenic phosphate and the temperature of early Ordovician seawater. *Palaios* **22**, 98–103.

Bendrey R., Vella D., Zazzo A., Balasse M. and Lepetz S. (2015) Exponentially decreasing tooth growth rate in horse teeth: implications for isotopic analyses. *Archaeometry* **57**, 1104–1124.

Blumenthal S. A., Cerling T. E., Chritz K. L., Bromage T. G., Kozdon R. and Valley J. W. (2014) Stable isotope time-series in mammalian teeth: in situ $\delta^{18}O$ from the innermost enamel layer. *Geochim. Cosmochim. Acta* **124**, 223–236.

Bryant D. J., Koch P. L., Froelich P. N., Showers W. J. and Genna B. J. (1996) Oxygen isotope partitioning between phosphate and carbonate in mammalian apatite. *Geochim. Cosmochim. Acta* **60**, 5145–5148.

Cerling T. E. and Sharp Z. D. (1996) Stable carbon and oxygen isotope analysis of fossil tooth enamel using laser ablation. *Palaeogeogr. Palaeoclimatol. Palaeoecol.* **126**, 173–186.

Chenery C., Mueldner G., Evans J., Eckardt H. and Lewis M. (2010) Strontium and stable isotope evidence for diet and mobility in roman Gloucester, UK. *J. Archaeol. Sci.* **37**, 150–163.

Cherniak D. (2000) Rare earth element diffusion in apatite. *Geochim. Cosmochim. Acta* **64**, 3871–3885.

Clementz M. T. (2012) New insight from old bones: stable isotope analysis of fossil mammals. *J. Mammal.* **93**, 368–380.

Driessens F. C. and Verbeeck R. (1990) *Biominerals*. CRC Press.

Elliott J. C. (2002) Calcium phosphate biominerals. *Rev. Mineral. Geochem.* **48**, 427–453.

Fox D. L. and Fisher D. C. (2001) Stable isotope ecology of a late miocene population of *gomphotherium productus* (mammalia, proboscidea) from port of entry pit, Oklahoma, USA. *Palaios* **16**, 279–293.

Fricke H. C. and O'Neil J. R. (1996) Inter-and intra-tooth variation in the oxygen isotope composition of mammalian tooth enamel phosphate: Implications for palaeoclimatological and palaeobiological research. *Palaeogeogr. Palaeoclimatol. Palaeoecol.* **126**, 91–99.

Fricke H. C., Clyde W. C. and O'Neil J. R. (1998) Intra-tooth variations in $\delta^{18}O$ (PO_4) of mammalian tooth enamel as a record of seasonal variations in continental climate variables. *Geochim. Cosmochim. Acta* **62**, 1839–1850.

Hiller C. R., Robinson C. and Weatherell J. A. (1975) Variations in the composition of developing rat incisor enamel. *Calcif. Tissue Res.* **18**, 1–12.

Hillson S. (1986) *Teeth*. Cambridge University Press, Cambridge, UK.

Holroyd P. A., Barrón-Ortiz C. R., Cammidge T., Rankin B. D. and Hoppe K. A. (2014) *Serial Sampling of Mammalian Enamel does not Equal Seasonal Sampling*. GSA Annual Meeting in Vancouver, British Columbia.

Hoppe K. A., Stover S. M., Pascoe J. R. and Amundson R. (2004) Tooth enamel biomineralization in extant horses: Implications for isotopic microsampling. *Palaeogeogr. Palaeoclimatol. Palaeoecol.* **206**, 355–365.

Kierdorf H. and Kierdorf U. (1997) Disturbances of the secretory stage of amelogenesis in fluorosed deer teeth: a scanning electron-microscopic study. *Cell Tissue Res.* **289**, 125–135.

Kierdorf H., Zeiler J. and Kierdorf U. (2006) Problems and pitfalls in the diagnosis of linear enamel hypoplasia in cheek teeth of cattle. *J. Archaeol. Sci.* **33**, 1690–1695.

Kierdorf H., Witzel C., Upex B., Dobney K. and Kierdorf U. (2012) Enamel hypoplasia in molars of sheep and goats, and its relationship to the pattern of tooth crown growth. *J. Anat.* **220**, 484–495.

Kierdorf H., Kierdorf U., Frölich K. and Witzel C. (2013) Lines of evidence–incremental markings in molar enamel of soay sheep as revealed by a fluorochrome labeling and backscattered electron imaging study. *PLoS One* **8**, e74597.

Koch P. L. (1998) Isotopic reconstruction of past continental environments. *Annu. Rev. Earth Planet. Sci.* **26**, 573–613.

Koch P. L. (2007) Isotopic study of the biology of modern and fossil vertebrates. In *Stable Isotopes in Ecology and Environmental Science* (eds. R. Michener and K. Lajtha). Blackwell Publishing, pp. 99–154.

Koch P., Tuross N. and Fogel M. (1997) The effects of sample treatment and diagenesis on the isotopic integrity of carbonate in biogenic hydroxylapatite. *J. Archaeol. Sci.* **24**, 417–429.

Koeingswald W. V., Martin T. and Pfretzschner H. U. (1993) Phylogenetic interpretations of enamel structures in mammalian teeth: possibilities and problems. In *Mammalian Phylogeny: Placentals* (eds. F. S. Szalay, M. J. Novacek and M. C. McKenna). Springer-Verlag, New York, pp. 303–314.

Koenigswald W. V. and Sander P. (1997) *Glossary of Terms used for Enamel Microstructures, Tooth Enamel Microstructure*. A.A. Balkema/Rotterdam/ Brookfield, pp. 267–280.

Kohn M. J. (2008) Models of diffusion-limited uptake of trace elements in fossils and rates of fossilization. *Geochim. Cosmochim. Acta* **72**, 3758–3770.

Kohn M. J. (2004) Comment: Tooth enamel mineralization in ungulates: Implications for recovering a primary isotopic time-series, by B.H. Passey and T.E. Cerling (2002). *Geochim. Cosmochim. Acta* **68**, 403–405.

Kohn M. J. and Cerling T. E. (2002) Stable isotope compositions of biological apatite. *Rev. Mineral. Geochem.* **48**, 455–488.

Kohn M. J., Schoeninger M. J. and Valley J. W. (1998) Variability in oxygen isotope compositions of herbivore teeth: reflections of seasonality or developmental physiology? *Chem. Geol.* **152**, 97–112.

Kohn M. J., Schoeninger M. J. and Barker W. W. (1999) Altered states: effects of diagenesis on fossil tooth chemistry. *Geochim. Cosmochim. Acta* **63**, 2737–2747.

Kohn M. J., Strömberg C. A., Madden R. H., Dunn R. E., Evans S., Palacios A. and Carlini A. A. (2015) Quasi-static eocene–oligocene climate in Patagonia promotes slow faunal evolution and mid-cenozoic global cooling. *Palaeogeogr. Palaeoclimatol. Palaeoecol.* **435**, 24–37.

Martin C., Bentaleb I., Kaandorp R., Iacumin P. and Chatri K. (2008) Intra-tooth study of modern rhinoceros enamel $d^{18}O$: is the difference between phosphate and carbonate $\delta^{18}O$ a sound diagenetic test? *Palaeogeogr. Palaeoclimatol. Palaeoecol.* **266**, 183–189.

Moss-Salentijn L., Moss M. and Yuan M. S.-T. (1997) The ontogeny of mammalian enamel. In *Tooth Enamel Microstructure* (eds. W. V. Koengswald and P. M. Sander), pp. 5–30. A.A. Balkema/ Rotterdam/ Brookfield.

O'Neil J. R., Roe L. J., Reinhard E. and Blake R. (1994) A rapid and precise method of oxygen isotope analysis of biogenic phosphate. *Israel J. Earth Sci.* **43**, 203–212.

Passey B. H. and Cerling T. E. (2002) Tooth enamel mineralization in ungulates: implications for recovering a primary isotopic time-series. *Geochim. Cosmochim. Acta* **66**, 3225–3234.

Passey B. H., Cerling T. E., Perkins M. E., Voorhies M. R., Harris J. M. and Tucker S. T. (2002) Environmental change in the great plains: an isotopic record from fossil horses. *J. Geol.* **110**, 123–140.

Passey B. H., Cerling T. E., Schuster G. T., Robinson T. F., Roeder B. L. and Krueger S. K. (2005) Inverse methods for estimating primary input signals from time-averaged isotope profiles. *Geochim. Cosmochim. Acta* **69**, 4101–4116.

Passey B. H., Cerling T. E. and Levine N. E. (2007) Temperature dependence of oxygen isotope acid fractionation for modern and fossil tooth enamels. *Rapid Commun. Mass Spectrom.* **21**, 2853–2859.

Pellegrini M., Lee-Thorp J. A. and Donahue R. E. (2011) Exploring the variation of the $\delta^{18}O_P$ and $\delta^{18}O_C$ relationship in enamel increments. *Palaeogeogr. Palaeoclimatol. Palaeoecol.* **310**, 71–83.

Pfretzschner H. (1992) Enamel microstructure and hypsodonty in large mammals. In *Structure, Function and Evolution of Teeth* (eds. P. Smith and E. Tchernov). Freund Publishing House Ltd., London and Tel Aviv, pp. 147–162.

Putnis A. (2002) Mineral replacement reactions: from macroscopic observations to microscopic mechanisms. *Mineral. Mag.* **66**, 689–708.

Robinson C., Hiller C. R. and Weatherell J. A. (1974) Uptake of ^{32}P-labelled phosphate into developing rat incisor enamel. *Calcif. Tissue Res.* **15**, 143–152.

Robinson C., Fuchs P., Deutsch D. and Weatherell J. (1978) Four chemically distinct stages in developing enamel from bovine incisor teeth. *Caries Res.* **12**, 1–11.

Robinson C., Briggs H., Atkinson P. and Weatherell J. (1979) Matrix and mineral changes in developing enamel. *J. Dent. Res.* **58**, 871–882.

Roche D., Ségalen L., Balan E. and Delattre S. (2010) Preservation assessment of Miocene-Pliocene tooth enamel from Tugen Hills (Kenyan Rift Valley) through FTIR, chemical and stable-isotope analyses. *J. Archaeol. Sci.* **37**, 1690–1699.

Stipp S. L., Hochella M. F., Parks G. A. and Leckie J. O. (1992) Cd^{2+} uptake by calcite, solid-state diffusion, and the formation of solid-solution: Interface processes observed with near-surface sensitive techniques (XPS, LEED, and AES). *Geochim. Cosmochim. Acta* **56**, 1941–1954.

Suga S. (1979) Comparative histology of progressive mineralization pattern of developing incisor enamel of rodents. *J. Dent. Res.* **58**, 1025–1026.

Suga S. (1982) Progressive mineralization pattern of developing enamel during the maturation stage. *J. Dent. Res.* **61**, 1532–1542.

Sydney-Zax M., Mayer I. and Deutsch D. (1991) Carbonate content in developing human and bovine enamel. *J. Dent. Res.* **70**, 913–916.

Tafforeau P., Bentaleb I., Jaeger J.-J. and Martin C. (2007) Nature of laminations and mineralization in rhinoceros enamel using histology and X-ray synchrotron microtomography: Potential implications for palaeoenvironmental isotopic studies. *Palaeogeogr. Palaeoclimatol. Palaeoecol.* **246**, 206–227.

Zazzo A., Lécuyer C., Sheppard S. M., Grandjean P. and Mariotti A. (2004) Diagenesis and the reconstruction of paleoenvironments: a method to restore original $\delta^{18}O$ values of carbonate and phosphate from fossil tooth enamel. *Geochim. Cosmochim. Acta* **68**, 2245–2258.

Zazzo A., Balasse M. and Patterson W. P. (2005) High-resolution $\delta^{13}C$ intratooth profiles in bovine enamel: implications for mineralization pattern and isotopic attenuation. *Geochim. Cosmochim. Acta* **69**, 3631–3642.

Zazzo A., Balasse M., Passey B. H., Moloney A. P., Monahan F. J. and Schmidt O. (2010) The isotope record of short-and long-term dietary changes in sheep tooth enamel: implications for quantitative reconstruction of paleodiets. *Geochim. Cosmochim. Acta* **74**, 3571–3586.

Zazzo A., Bendrey R., Vella D., Moloney A. P., Monahan F. J. and Schmidt O. (2012) A refined sampling strategy for intra-tooth stable isotope analysis of mammalian enamel. *Geochim. Cosmochim. Acta* **84**, 1–13.

Associate editor: Marc Norman